# ANALYSIS FOR VELOCITY-DEPENDENT CONTACT ANGLE HYSTERESIS ON ROUGH SURFACE[*]

XIANMIN XU[†], YINYU ZHAO[‡], AND XIAOPING WANG[§]

**Abstract.** Contact angle hysteresis is an interesting phenomenon in wetting. While it is believed that roughness or chemically inhomogeneity of the solid surface can cause the phenomenon, quantitative study of the problem is difficult. In this paper, we use a phase field equation with a relaxed boundary condition on a rough boundary to model contact angle hysteresis. By asymptotic analysis, we derive an ordinary differential system for the apparent contact angle and the contact point. Numerical examples show that the ordinary differential equation can be used to understand the contact angle hysteresis, including the asymmetric dependence of the advancing and receding contact angles on velocity, which is observed recently in experiments.

**Key words.** Contact angle hysteresis, phase field equation, asymptotic analysis

**AMS subject classifications.** 41A60,49Q05,76T10

**1. Introduction.** Contact angle hysteresis is an interesting phenomenon in wetting problem[6, 7, 3]. When a liquid is moving on a solid surface, the advancing angle is usually different from the receding angle, as shown in Figure 1.1. This is called contact angle hysteresis(CAH). CAH is an unsolved problem in fluid dynamics[10, 19, 17, 22]. In general, CAH is believed to be mainly induced by the roughness or inhomogeneity of the solid surface, although there exists slight hysteresis even on atomically smooth surface. However, quantitative understanding of the phenomenon is still on the way, especially for the case that CAH might depend on velocity[12].
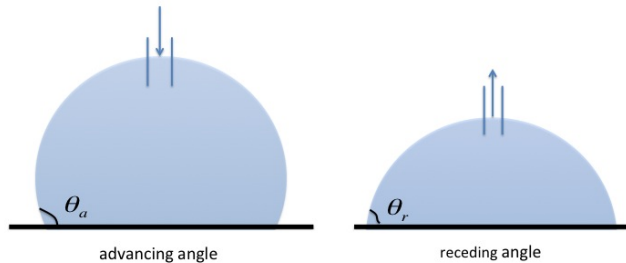


FIG. 1.1. *Contact angle hysteresis: the advancing angle is larger than the receding angle.*

Physical study of the CAH problem has been done extensively[3]. There are plenty of experiments on various properties of CAH and also on its many applications in

[†]LSEC, ICMSEC, Academy of Mathematics and Systems Science, Chinese Academy of Sciences, Beijing 100190, China; School of Mathematical Sciences, University of Chinese Academy of Sciences, Beijing 100049, China, (xmxu@lsec.cc.ac.cn), Corresponding author.

[‡]LSEC, ICMSEC, Academy of Mathematics and Systems Science, Chinese Academy of Sciences, Beijing 100190, China, (zhaoyinyu@lsec.cc.ac.cn).

[§]Department of Mathematics, the Hong Kong University of Science and Technology, Clear Water Bay, Kowloon, Hong Kong, China, (mawang@ust.hk).

1

biology and technology[16, 21, 17, 31, 12]. Theoretical analysis of the problem is quite complicated. Most studies concentrate on the quasi-static process of CAH[11, 26]. The study on the dynamic CAH is limited to a few cases with special geometric or chemical properties of the solid surface. For example, Joanny and de Gennes considered a smooth surface with very dilute defects so that the analysis for pinning of the contact line by one defect can be applied[13].

From the mathematical point of view, theoretical study of CAH is also very challenging. It is not only because this is a difficult moving contact line problem[2], but also because its multiscale feature that microscopic roughness or inhomogeneity of the solid surface might affect the macroscopic properties of the contact angle. Due to the complication of the problem, mathematical analysis of CAH mainly focuses on a simplified problem without flow effect. Then the problem will be modelled by minimizing the total surface energy in the system. The existence of many local minimizers of the energy minimization problem has been analyzed in [14, 4] and this can be used to understand CAH. In [1, 8, 23], some effective models are derived assuming an energy barrier when minimizing the energy. In [29], we did analysis for a quasi-static proces of CAH for a two-dimensional problem with chemically inhomogeneous surfaces. This can be generalized to the three dimensional case by using a modified Wenzel and Cassie equation[30, 27]. To study the velocity dependence of CAH, we study a phase-field model with relaxed boundary condition on chemically-patterned surfaces[25].

In this paper, we generalize the analysis in [25] to a more general situation that the solid surface could be both geometrically rough and chemically inhomogeneous. We consider a phase-field boundary equation with a relaxed boundary condition. To study the velocity dependence, we assume the solid boundary is moving with some given velocity. We derive the sharp-interface limit of the phase-field equation by asymptotic analysis. The dynamics for the contact point and the apparent contact angle are derived from the the sharp-interface limit. It is a much complicated ordinary differential system. The system can be reduced to the one in [25] when the geometrical roughness does not appear. By solving the ordinary differential system numerically, we observe the clear CAH behavior for various rough surfaces. Interestingly, the system can give quite similar phenomena of asymmetric dependence of CAH on velocity to that in experiments[12]. This indicates that our analysis captures some essential features of CAH.

The structure of the paper is as follows. In Section 2, we introduce the phase-field model for the wetting problem. In Section 3, asymptotic analysis is given to derive the sharp interface limit of the phase field equation. An ordinary differential system for the apparent contact angle and the contact points is derived in Section 4. Some numerical examples are illustrated in Section 5. Conclusions and a few discussions are given in the last section.

**2. The phase field model for wetting problem.** We consider a two-phase flow in a channel with geometrically rough boundary as shown in Figure 2.1. The upper and lower boundaries are given by $y = \pm(h_0 + \delta H(\frac{x}{\delta}))$. Here $H(\cdot)$ is a periodic and differentiable function. Here $\delta \ll h_0$ is a small positive number. We assume that the boundary might also be chemically inhomogeneous in the sense that the Young's angle $\theta_Y$, which is the static contact angle of a liquid on a flat surface, is not a constant on the boundary. For simplicity, we assume $\theta_Y(x)$ is also a periodic function with period $\delta$. Suppose the average horizontal velocity of the fluid is $U$. For convenience, we choose a frame moving with velocity $U$, and consider the problem in a domain
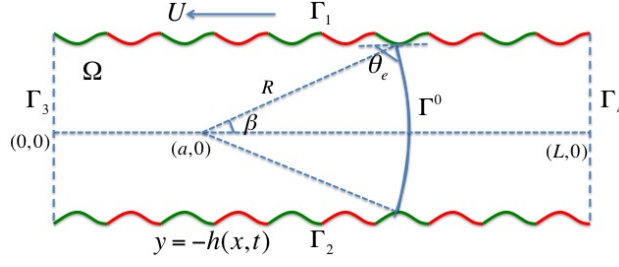
FIG. 2.1. *A free interface in a channel with periodically rough and inhomogeneous surface.*

$\Omega(t)$, whose boundaries moves with a velocity $-U$ horizontally. The domain $\Omega(t)$ is given by

$$\Omega(t) = (0, L) \times (-h(x, t), h(x, t)), \qquad (2.1)$$

with $h(x, t) = h_0 + \delta H((x + Ut)/\delta)$. We assume $L/\varepsilon$ is an integer so that the volume of $\Omega(t)$ does not change with time.

On rough of chemically patterned surface, the interface will oscillates due to the stick-slip behaviours of the contact points[24]. The problem is quite complicated due to the existence of the moving contact line and the microscopic roughness of the boundary. In general, the moving contact line problem can be modelled by a coupled Navier-Stokes-Cahn-Hilliard system with a generalized Navier slip boundary condition[18]. When the fluid velocity is small, one can ignore the fluid effect and use a Cahn-Hilliard equation with a relaxed boundary condition to model the evolution of the contact angle[5]. To study the evolution of the contact angle, we consider the following Cahn-Hilliard equation,

$$\begin{cases} \varepsilon \phi_t = \Delta \mu \\ \mu = -\varepsilon \Delta \phi + \frac{F'(\phi)}{\varepsilon} \end{cases} \qquad (2.2)$$

with an initial condition $\phi(x, 0) = \phi_0(x)$. Here $\phi$ is the phase-field function, $\mu$ is the chemical potential, and $F(\phi) = \frac{(1-\phi^2)^2}{4}$ is the free energy density. The parameter $\varepsilon \ll \delta$ measures the interface thickness. The boundary condition on the upper and lower boundary $\Gamma_{1,2} := \{(x, y)|y = \pm h(x, t), 0 < x < L\}$ are given by

$$\partial_n \mu = 0, \ \varepsilon(\phi_t + u_{w,\tau} \partial_\tau \phi) = -\alpha(\varepsilon \partial_n \phi + \gamma'(x, t, \phi)). \qquad (2.3)$$

Here the normal derivative $\partial_n = \mathbf{n} \cdot \nabla$ and $\mathbf{n}$ is the unit exterior normal to the boundary of $\Omega$; $\tau$ is the unit tangential direction of the boundary pointing right and $u_{w,\tau} = (-U, 0) \cdot \tau$ is the tangential velocity of the wall; $\alpha$ is a relaxation parameter. The surface energy $\gamma(x, t, \phi) = \frac{\gamma_{SV} - \gamma_{SL}}{2} - \frac{\gamma_{SV} - \gamma_{SL}}{4}(3\phi - \phi^3)$. By Young's equation $\gamma_{SV} - \gamma_{SL} = \sigma \cos \theta_Y$ with the Young's angle $\theta_Y(x + Ut)$, it can be simplified as

$$\gamma(x, t, \phi) = \frac{\gamma_{SV} - \gamma_{SL}}{2} - \frac{\sigma \cos \theta_Y(x + Ut)}{4}(3\phi - \phi^3).$$

Here $\sigma = \frac{2\sqrt{2}}{3}$ is the (dimensionless) liquid-vapor surface tension[29]. In addition, we use the notation $\gamma'(x, t, \phi) = \frac{\partial \gamma}{\partial \phi}$. The boundary conditions on the left and right

boundaries $\Gamma_{3,4} = \{(x,y)| - h(x,t) < y < h(x,t), x = 0, L\}$ are given by

$$\partial_n \mu = 0, \phi = 1, \qquad\qquad \text{on } \Gamma_3, \qquad\qquad (2.4)$$
$$\partial_n \mu = 0, \phi = -1, \qquad\quad \text{on } \Gamma_4. \qquad\qquad (2.5)$$

Here we assume $\phi = 1$ in the liquid domain and $\phi = -1$ in the vapor domain.

**3. Sharp-interface limit of the phase field model.** We study the sharp-interface limit of the system (2.2)-(2.5) by asymptotic matching method. In this section, we will use a notation $\mathbf{x} = (x,y)$ to represent the coordinate of a point in $\Omega$.

**3.1. The bulk equation.** *Outer expansions.* We first consider the asymptotic expansion of the equation (2.2) far from the two-phase interface $\Gamma^\varepsilon(t)$. Suppose the lead order approximation of $\Gamma^\varepsilon(t)$ is $\Gamma^0(t)$. The domain $\Omega$ is divided by $\Gamma^0$ into two parts $\Omega^+$ and $\Omega^-$. Suppose

$$\phi^\pm = \phi_0^\pm + \varepsilon \phi_1^\pm + \cdots, \qquad\qquad \text{in } \Omega^\pm, \qquad\qquad (3.1)$$
$$\mu^\pm = \varepsilon^{-1} \mu_{-1}^\pm + \mu_0^\pm + \varepsilon \mu_1^\pm + \cdots, \qquad \text{in } \Omega^\pm. \qquad\qquad (3.2)$$

Here we let $\phi_0^+$ to be positive and $\phi_0^-$ negative. Substitute the above expansions into the equation (2.2). The leading order is given by

$$O(\varepsilon^{-1}): \qquad \Delta \mu_{-1}^\pm = 0, \quad \mu_{-1}^\pm = F'(\phi_0^\pm) = (\phi_0^\pm)^3 - \phi_0^\pm, \qquad\qquad (3.3)$$

and the next order is

$$O(1): \qquad \Delta \mu_0^\pm = 0, \quad \mu_0^\pm = (3(\phi_0^\pm)^2 - 1)\phi_1^\pm. \qquad\qquad (3.4)$$

Substitute the expansions to the boundary condition, we obtain

$$\partial_n \mu_{-1}^\pm = 0, \quad \partial_n \mu_0^\pm = 0, \qquad \text{on } \partial\Omega^\pm, \qquad\qquad (3.5)$$
$$\phi_0^+ = 1, \qquad\qquad\qquad \text{on } \Gamma_3, \qquad\qquad (3.6)$$
$$\phi_0^- = -1, \qquad\qquad\qquad \text{on } \Gamma_4, \qquad\qquad (3.7)$$
$$\gamma'(\phi_0^\pm) = 0 \qquad\qquad \text{on } \partial\Omega^\pm \cap (\Gamma_1 \cup \Gamma_2). \qquad\qquad (3.8)$$

*Inner expansions.* To analyse the sharp-interface limit of the Cahn-Hilliard equation, we need consider the inner expansions near the interface $\Gamma^0$. For that purpose, we denote $d(\mathbf{x})$ the signed distance function to $\Gamma^0$ and let $d(\mathbf{x}) < 0$ in $\Omega^-$ and $d(\mathbf{x}) > 0$ in $\Omega^+$. Then the unit normal of $\Gamma^0$ and the signed distance curvature $\kappa$ of the interface is given by

$$\mathbf{n} = \nabla d, \qquad \kappa = \Delta d. \qquad\qquad (3.9)$$

It is easy to see that $\mathbf{n}$ is the unit normal pointing into $\Omega^+$ and $\kappa(\mathbf{x})$ is positive when $\Omega^-$ is convex near $\mathbf{x}$. We introduce a stretched variable near the interface $\Gamma^0$,

$$\xi = \frac{d(\mathbf{x})}{\varepsilon}.$$

Assume that $\phi$ and $\mu$ can be written in variables $(\mathbf{x}, \xi, t)$ with expansions,

$$\phi = \tilde{\phi}_0(\mathbf{x}, \xi, t) + \varepsilon \tilde{\phi}_1(\mathbf{x}, \xi, t) + \cdots, \qquad\qquad (3.10)$$
$$\mu = \varepsilon^{-1} \tilde{\mu}_{-1}(\mathbf{x}, \xi, t) + \tilde{\mu}_0(\mathbf{x}, \xi, t) + \cdots. \qquad\qquad (3.11)$$

In the new coordinates, the derivative can be rewritten as

$$\nabla = \nabla_{\mathbf{x}} + \varepsilon^{-1}\mathbf{n}\partial_\xi,$$
$$\Delta = \varepsilon^{-2}\partial_{\xi\xi} + \varepsilon^{-1}\kappa\partial_\xi + \Delta_{\mathbf{x}} + 2\mathbf{n}\cdot\nabla_{\mathbf{x}}\partial_\xi.$$

We substitute the expansions (3.10)-(3.11) into the equation (2.2) and use the above expressions for derivatives. In leading order, we have

$$\partial_{\xi\xi}\tilde{\mu}_{-1} = 0, \qquad \tilde{\mu}_{-1} = -\partial_{\xi\xi}\tilde{\phi}_0 + F'(\tilde{\phi}_0), \tag{3.12}$$

and the next order is

$$\partial_{\xi\xi}\tilde{\mu}_0 = 0, \qquad \tilde{\mu}_0 = -\partial_{\xi\xi}\tilde{\phi}_1 + \kappa\partial_\xi\tilde{\phi}_0 + 2(\mathbf{n}\cdot\nabla_{\mathbf{x}})\partial_\xi\tilde{\phi}_0 + F''(\tilde{\phi}_0)\tilde{\phi}_1. \tag{3.13}$$

We might also have the next order expansion for $\tilde{\mu}_1$ that

$$\partial_{\xi\xi}\tilde{\mu}_1 = 0.$$

By the first equation of (3.12), we have

$$\tilde{\mu}_{-1} = c_0\xi + c_1. \tag{3.14}$$

Using the matching condition for $\lim_{\xi\to\pm\infty}\tilde{\mu}_{-1} = \mu_{-1}^{\pm}$ and the boundedness of $\mu_{-1}^{\pm}$, we obtain $c_0 = 0$ and

$$\mu_{-1}^{\pm} = c_1, \qquad \text{on } \Gamma^0. \tag{3.15}$$

That means $\mu_{-1}^{\pm}$ is continuous across $\Gamma^0$. Similarly, by the first equation of (3.13) and the matching condition of $\tilde{\mu}_0$, we know $\tilde{\mu}_0$ is independent of $\xi$ and $\mu_0^{\pm}$ is continuous across $\Gamma^0$. In addition, by the matching condition that

$$\lim_{\xi\to\pm\infty}\partial_\xi\tilde{\mu}_0 = \lim_{d(\mathbf{x})\to\pm 0}\mathbf{n}\cdot\nabla_{\mathbf{x}}\mu_{-1}(\mathbf{x}). \tag{3.16}$$

We have $\mathbf{n}\cdot\nabla\mu_{-1} = 0$ on $\Gamma^0$. Combining with (3.3) that $\Delta\mu_{-1}^{\pm} = 0$, we thus have $\mu_{-1}^{\pm}$ are both constant functions such that

$$\mu_{-1}^{\pm} = c_1, \qquad \text{in } \Omega^{\pm}.$$

This implies that $\mu_{-1}$ is constant in the whole domain $\Omega$. Similar arguments lead to the fact that $\mu_0$ is a constant in $\Omega$.

Noticing that $\mu_{-1}^{\pm} = (\phi_0^{\pm})^3 - \phi_0^{\pm}$ and the boundary condition (3.6)-(3.7) on $\Gamma_3$ and $\Gamma_4$, we have

$$\mu_{-1}^{\pm} = c_1 = 0, \qquad \text{in } \Omega^{\pm}, \tag{3.17}$$

and

$$\phi_0^{\pm}(\mathbf{x}) = \pm 1, \qquad \mathbf{x} \in \Omega^{\pm}(t). \tag{3.18}$$

By the formula for $\tilde{\mu}_{-1}$ in (3.12), we have

$$-\partial_{\xi\xi}\tilde{\phi}_0 + F'(\tilde{\phi}_0) = 0. \tag{3.19}$$

Using the matching condition for $\tilde{\phi}_0$ that $\lim_{\xi \to \pm\infty} \tilde{\phi}_0 = \phi_0^{\pm} = \pm 1$, we know that the above equation has a unique solution $\tilde{\phi}_0 = \Phi(\xi) := \tanh(\frac{\xi}{\sqrt{2}})$. Here we use the fact that $F'(\tilde{\phi}_0) = \tilde{\phi}_0^3 - \tilde{\phi}_0$.

By the formula for $\tilde{\mu}_0$ and the fact that $\tilde{\mu}_0 = \mu_0$ is a constant, we have

$$\mu_0 = -\partial_{\xi\xi}\tilde{\phi}_1 + \kappa \partial_\xi \tilde{\phi}_0 + F''(\tilde{\phi}_0)\tilde{\phi}_1 \tag{3.20}$$

Multiply $\partial_\xi \tilde{\phi}_0$ to the above equation, notice also that $\tilde{\phi}_0$ satisfies (3.19), we obtain

$$2\mu_0 = \kappa \int_{-\infty}^{+\infty} (\partial_\xi \tilde{\phi}_0)^2 d\xi = \kappa\sigma \tag{3.21}$$

with $\sigma = \int_{-\infty}^{+\infty} (\partial_\xi \tilde{\phi}_0)^2 d\xi = \frac{2\sqrt{2}}{3}$. This implies that $\kappa$ is a constant(since $\mu_0$ is constant). In other words, the interface $\Gamma_0$ has constant curvature at any time. We would like to remark that the leading order equation (3.21) is different from that of the standard Cahn-Hilliard equation[15, 5]. This is because we choose a time scaling which leads to a very fast evolution of the Cahn-Hilliard equation to its equilibrium state. In this time scale, we only observe the evolution of an interface with constant curvature. We will use this fact to do asymptotic analysis near the contact point in the following subsection.

**3.2. Asymptotic analysis near the contact point.** From the analysis above, we see that the curvature of $\Gamma^0$ is a constant changing with time. By symmetry of the channel with respect to the central line $y = 0$, we can assume that the limiting interface $\Gamma^0$ is a circle centered at $(a(t), 0)$ with radius $R(t)$(as shown in Figure 2.1):

$$\Gamma^0(t) := \{(a(t), 0) + R(t)(\cos\vartheta, \sin\vartheta); |\vartheta| \leq \beta(t)\}. \tag{3.22}$$

Suppose the zero level set of $\phi_\varepsilon$ is given by

$$\Gamma^\varepsilon(t) := \{(a(t), 0) + R^\varepsilon(\vartheta, t)(\cos\vartheta, \sin\vartheta); |\vartheta| \leq \beta^\varepsilon(t)\}. \tag{3.23}$$

We can assume the expansion

$$R^\varepsilon(\vartheta, t) = R(t) + \varepsilon R_1(\vartheta, t) + \varepsilon^2 R_2(\vartheta, t) + \cdots. \tag{3.24}$$

Near the contact point on $\Gamma_1$, we consider the stretched variables

$$\xi = \frac{R(t) - r}{\varepsilon}, \qquad \eta = \frac{d_\Gamma(\mathbf{x})}{\varepsilon}, \tag{3.25}$$

with $\mathbf{x} = (x, y)$ and $r = \sqrt{(x - a(t))^2 + y^2}$. Here $d_\Gamma$ is the signed distance function to the upper boundary $\Gamma_1$ of $\Omega_\varepsilon$, and $d_\Gamma(x, y) < 0$ for $y < h(x, t)$. In addition, we have $\vartheta = \arctan\frac{y}{x - a(t)}$.

Denote $\phi(\mathbf{x}, t) = \hat{\phi}(\xi, \eta, t)$ and let $\mathbf{n}_\Gamma$ be the outer normal of $\Gamma_1$ and $\mathbf{n}_\vartheta$ be the normal of $\Gamma^0$ pointing into $\Omega^+$. It is easy to see that

$$\mathbf{n}_\Gamma = \nabla d_\Gamma \qquad \text{and} \qquad \mathbf{n}_\vartheta = -(\cos\vartheta, \sin\vartheta)^T. \tag{3.26}$$

By these notations, we easily have

$$\nabla\phi = \varepsilon^{-1}\partial_\eta \hat{\phi}\mathbf{n}_\Gamma + \varepsilon^{-1}\partial_\xi \hat{\phi}\mathbf{n}_\vartheta, \tag{3.27}$$

$$\Delta\phi = \varepsilon^{-2}\partial_{\eta\eta}\hat{\phi} + 2\varepsilon^{-2}\mathbf{n}_\Gamma \cdot \mathbf{n}_\vartheta \partial_{\eta\xi}\hat{\phi} + \varepsilon^{-2}\partial_{\xi\xi}\hat{\phi}, \tag{3.28}$$

$$\phi_t = \varepsilon^{-1}(\dot{R} + \dot{a}\cos\vartheta)\partial_\xi \hat{\phi} + \partial_t \hat{\phi}. \tag{3.29}$$

Here $\dot{R} = \frac{dR(t)}{dt}$ and $\dot{a}$ is similarly defined. Assume $\hat{\phi}$ has the following expansion,

$$\hat{\phi} = \hat{\phi}^0(\xi, \eta, t) + \varepsilon \hat{\phi}^1(\xi, \eta, t) + \cdots. \tag{3.30}$$

Substitute the expansion to the equation (2.2) and the boundary condition (2.3). The leading order of the expansion gives

$$\begin{cases} \hat{\phi}^0_{\eta\eta} + 2\mathbf{n}_\Gamma \cdot \mathbf{n}_\vartheta \hat{\phi}^0_{\eta\xi} + \hat{\phi}^0_{\xi\xi} - F'(\hat{\phi}^0) = 0, & \text{when } \eta > 0 \\ (\dot{R} + \dot{a}\cos\beta + u_{w,\tau}\tau \cdot \mathbf{n}_\beta + \alpha\mathbf{n}_\Gamma \cdot \mathbf{n}_\beta)\hat{\phi}^0_\xi = -\alpha(\hat{\phi}^0_\eta + \gamma'(x_{ct}, t, \hat{\phi}^0)), & \text{when } \eta = 0. \end{cases} \tag{3.31}$$

Here $x_{ct}$ is the $x$-coordinate of the contact point. We also have the matching condition that

$$\lim_{\eta \to +\infty} \hat{\phi}^0(\xi, \eta, t) = \tilde{\phi}_0(\xi, t). \tag{3.32}$$

It is easy to see that $\hat{\phi}^0(\xi, \eta, t) = \Phi(\xi)$ is the solution of the first equation. Notice that

$$\gamma'(\hat{\phi}^0) = \frac{3\sigma}{4}((\hat{\phi}^0)^2 - 1)\cos\theta_Y = -\cos\theta_Y \partial_\xi \Phi = -\cos\theta_Y \hat{\phi}^0_\xi. \tag{3.33}$$

Here $\theta_Y$ represents $\theta_Y(x_{ct} + Ut)$. The second equation of (3.31) gives

$$\dot{R} + \dot{a}\cos\beta = -\alpha(\mathbf{n}_\Gamma \cdot \mathbf{n}_\beta - \cos(\theta_Y)) - u_{w,\tau}\tau \cdot \mathbf{n}_\beta. \tag{3.34}$$

The equation gives a relation of $R(t)$, $a(t)$ and $\beta(t)$. We specify some notations in the above equation: $\tau = \frac{1}{\sqrt{1+(\partial_x h)^2}}(1, \partial_x h)^T$ and $\mathbf{n}_\Gamma = \frac{1}{\sqrt{1+(\partial_x h)^2}}(-\partial_x h, 1)^T$. Using the notation of the dynamic contact angle $\theta_d$ which satisfies $\cos\theta_d = \mathbf{n}_\Gamma \cdot \mathbf{n}_\beta$ and $\theta_d \in (0, \pi)$, the equation could be simplified as

$$\dot{R} + \dot{a}\cos\beta = \alpha(\cos(\theta_Y) - \cos\theta_d) + u_{w,\tau}\sin\theta_d. \tag{3.35}$$

**4. Dynamics of the contact angle.** By the above analysis, the leading order of the Cahn-Hilliard equation gives a circular interface which satisfies the condition (3.35) at the contact point. In the following, we will use the property to derive a dynamics for the apparent contact angle and the contact point. The apparent contact angle is the angle between the interface and the homogenized solid boundary as shown in Figure 2.1.

We first notice that the Cahn-Hilliard equation satisfies the following mass conservation property

$$\frac{d}{dt}\int_\Omega \phi dx = 0. \tag{4.1}$$

This can be obtained by integration of the first equation of (2.2) and use the homogeneous Neumann boundary condition of $\mu$. The leading order of the equation (4.1) leads to

$$\frac{d}{dt}\int_\Omega \phi_0 dx = 0, \text{ or equivalently } (|\Omega^+| - |\Omega^-|) = const. \tag{4.2}$$

Noticing that $|\Omega^+| + |\Omega^-| = |\Omega| = const$, we have the volume of both $\Omega^+$ and $\Omega^-$ are preserving. Denote $A$ as the volume of $\Omega^+$. It is easy to compute that

$$A = R^2(\beta - \sin\beta\cos\beta) + 2\int_0^{x_{ct}} h(x, t)dx \tag{4.3}$$

where $x_{ct}$ is the $x$-coordinate of the contact point. We also have the following geometric relation

$$R \sin \beta = h(x_{ct}, t), \qquad x_{ct} = a + R(t) \cos \beta. \tag{4.4}$$

We will use the equations (3.35), (4.3) and (4.4) to derive an ordinary differential equation for $\beta$ and $x_{ct}$.

By the equation (4.3), using $\frac{dA}{dt} = 0$, we have

$$R\dot{R}(\beta - \sin \beta \cos \beta) + R^2 \sin^2 \beta \dot{\beta} + h(x_{ct}, t)\dot{x}_{ct} + \int_0^{x_{ct}} \partial_t h(x, t) dx = 0. \tag{4.5}$$

The time derivative of the equation (4.4) gives

$$\dot{R} \sin \beta + (R \cos \beta)\dot{\beta} = \partial_x h(x_{ct}, t)\dot{x}_{ct} + \partial_t h(x_{ct}, t) \tag{4.6}$$

$$\dot{a} + \dot{R} \cos \beta - (R \sin \beta)\dot{\beta} = \dot{x}_{ct}. \tag{4.7}$$

Multiply (4.6) by $\sin \beta$ and (4.7) by $\cos \theta$ and add them together, then we obtain

$$\dot{R} + \dot{a} \cos \beta = \dot{x}_{ct}[\cos \beta + \partial_x h(x_{ct}, t) \sin \beta] + \partial_t h(x_{ct}, t) \sin \beta. \tag{4.8}$$

Substituting (4.8) into (3.35) and simple computations lead to

$$\dot{x}_{ct} = \frac{\alpha(\cos \theta_Y (x_{ct} + Ut) - \cos \theta_d) + u_{w,\tau} \sin \theta_d - \partial_t h(x_{ct}, t) \sin \beta}{\cos \beta + \partial_x h(x_{ct}, t) \sin \beta}. \tag{4.9}$$

This is an ordinary differential equation of the contact point $x_{ct}$, which depends on the unknown $\beta$. In the following, we will derive the equation of $\beta$. Using the first equation of (4.4), the equation (4.5) is reduced to

$$\dot{R}h(x_{ct}, t)\frac{\beta - \sin \beta \cos \beta}{\sin \beta} + h^2(x_{ct}, t)\dot{\beta} + h(x_{ct}, t)\dot{x}_{ct} + \int_0^{x_{ct}} \partial_t h(x, t) dx = 0. \tag{4.10}$$

Combing with the equation (4.6) and using the first equation of of (4.4), we can eliminate $\dot{R}$ and obtain by direct calculations that

$$\dot{\beta} = -g(\beta)\left[\frac{\sin^2 \beta + (\beta - \sin \beta \cos \beta)\partial_x h(x_{ct}, t)}{h(x_{ct}, t)}\dot{x}_{ct}\right.$$
$$\left. + \frac{(\beta - \sin \beta \cos \beta)\partial_t h(x_{ct}, t)}{h(x_{ct}, t)} + \frac{\sin^2 \beta}{h^2(x_{ct}, t)}\int_0^{x_{ct}} \partial_t h(x, t) dx\right], \tag{4.11}$$

where $g(\beta) = \frac{\sin \beta}{\sin \beta - \beta \cos \beta}$. The equations (4.9) and (4.11) compose a complete system to describe the dynamics of the contact point and $\beta$, noticing the following formula on dynamic contact angle

$$\cos \theta_d = \mathbf{n}_\Gamma \cdot \mathbf{n}_\beta = \frac{\partial_x h(x_{ct}, t) \cos \beta - \sin \beta}{\sqrt{1 + (\partial_x h(x_{ct}, t))^2}},$$

$$\sin \theta_d = -\tau \cdot \mathbf{n}_\beta = \frac{\partial_x h(x_{ct}, t) \sin \beta + \cos \beta}{\sqrt{1 + (\partial_x h(x_{ct}, t))^2}}.$$

Assume the parameter $\delta$ is small in the formula of $h(x, t)$, the rough boundary $y = h(x, t)$ approximates to an effective flat boundary $y = h_0$. Then the apparent
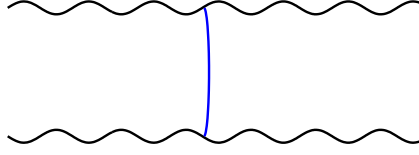
FIG. 5.1. *The channel with smooth oscillating boundaries.*

contact angle will be $\theta_a = \beta + \frac{\pi}{2}$ (see Figure 2.1). Then the equations (4.9) and (4.11) could be reduced to a system on $\theta_a$ and $x_{ct}$. Using the formula for $u_{w,\tau}$, direct calculations give

$$
\begin{cases}
\dot{x}_{ct} = \frac{\alpha(\cos\theta_Y(x_{ct}+Ut)-\cos\theta_d)}{\sin\theta_a - H'_{ct}\cos\theta_a} - \Big[\frac{1}{1+(H'_{ct})^2} - \frac{H'_{ct}\cos\theta_a}{\sin\theta_a - H'_{ct}\cos\theta_a}\Big]U \\[2ex]
\dot{\theta}_a = -\frac{\tilde{g}(\theta_a)}{h_{ct}}\Big[\big(\tilde{f}(\theta_a)+\cos^2\theta_a\big)\dot{x}_{ct} + \big(\tilde{f}(\theta_a)+\frac{\cos^2\theta_a}{h_{ct}}\int_0^{x_{ct}}H'(\frac{x+Ut}{\delta})dx\big)U\Big].
\end{cases}
$$
$$(4.12)$$

where we use the notations

$$
H'_{ct} = H'(\frac{x_{ct}+Ut}{\delta}), \qquad\qquad h_{ct} = h_0 + \delta H(\frac{x_{ct}+Ut}{\delta}),
$$

$$
\tilde{g}(\theta_a) = \frac{\cos\theta_a}{\cos\theta_a + (\theta_a-\frac{\pi}{2})\sin\theta_a}, \quad \tilde{f}(\theta_a) = (\theta_a - \frac{\pi}{2} + \sin\theta_a\cos\theta_a)H'(\frac{x_{ct}+Ut}{\delta}).
$$

Notice that when the boundary is flat so that $h = h_0$, the above equation is reduced to

$$
\begin{cases}
\dot{x}_{ct} = \frac{\alpha(\cos\theta_Y(x_{ct}+Ut)-\cos\theta_d)}{\sin\theta_a} - U \\[1ex]
\dot{\theta}_a = -\frac{\cos^3\theta_a}{\cos\theta_a+(\theta_a-\frac{\pi}{2})\sin\theta_a}\frac{\dot{x}_{ct}}{h_0}.
\end{cases}
$$

If we denote $\hat{x}_{ct} = x_{ct} + Ut$, the actual contact point on the boundary, the equation is reduced to

$$
\begin{cases}
\dot{\hat{x}}_{ct} = \frac{\alpha(\cos\theta_Y(\hat{x}_{ct})-\cos\theta_a)}{\sin\theta_a}, \\[1ex]
\dot{\theta}_a = -\frac{\cos^3\theta_a}{\cos\theta_a+(\theta_a-\frac{\pi}{2})\sin\theta_a}\frac{\dot{\hat{x}}_{ct}+U}{h_0}.
\end{cases}
$$

This is the same as the equation derived in [25].

**5. Numerical examples.** In this section, we will give some numerical examples to show that the ODE system (4.12) could be used to understand the interesting contact angle hysteresis phenomena.

*Example 1.* In the first example, we consider a smoothly oscillating boundary as shown in Figure 5.1. The boundary is given by $h(x,t) = h_0 + \delta H((x+Ut)/\delta)$, we set $h_0 = 0.8$, $H = \frac{\sin x}{4}$ and $U = \pm 0.01$. We did experiments for several choice of $\delta$. We choose $\theta_Y = \frac{\pi}{3}$. We solve the ODE system (4.12) numerically. Some typical numerical results are given in Figure 5.2.

In every subplot, we draw two curves on the trajectories of the solution of the ODE system in phase plane. Here we show the apparent contact angle with respect to the actual position $\hat{x}_{ct}$ of the contact point on the rough boundary. The lower curve

(a) $\delta = 0.04$

(b) $\delta = 0.02$

(c) $\delta = 0.01$

(d) $\delta = 0.005$
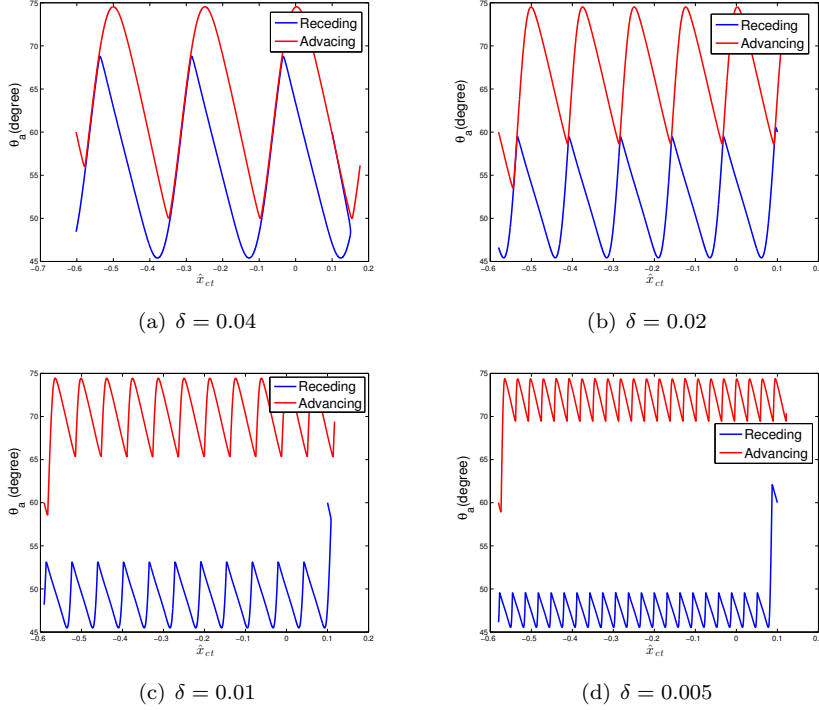
FIG. 5.2. *The apparent contact angle $\theta_a$ and the x-coordinate of the contact point $\hat{x}_{ct}$ in a channel with different oscillating rough boundary.*

corresponds to a negative velocity $U$ and the upper one corresponds to a positive $U$. When $U < 0$, the boundary moves to the right and we observe a receding contact angle. Similarly, when $U > 0$, we observe an advancing contact angle. For the case that $\delta = 0.04$, the period of the oscillation of the boundary is relatively large. We could see that the two trajectories overlap and the intervals of the advancing angle and receding angle are almost the same. One can hardly observe the contact angle hysteresis. On the other hand, when $\delta$ becomes smaller, which means that the boundary is more oscillating, the contact angle hysteresis becomes more obvious. When $\delta = 0.005$, we can see that the maximal advancing angle is about $74^o$ and minimal receding contact angle is about $46^o$. By the modified Wenel's equation [27], the maximal/minimal apparent contact angle of a liquid(in equilibrium) on an oscillating boundary is equal to $\theta_Y \pm \theta_g$, with $\theta_g$ being the largest angle of inclination of the boundary. In this example, the largest slope of the rough boundary is $1/4$ and so that $\theta_g = \arctan(1/4) \approx 14.04^o$. This means that with small velocity $U = 0.01$, the advancing angle and the receding angle approaches respectively to the maximal and receding apparent contact angles in equilibrium.

*Example 2.* In the second example, We consider a tube with nonsmooth oscillating rough boundaries. For simplicity, we choose a serrated shape of the boundary as shown Figure 5.3. We could define $h(x, t) = h_0 + \delta H((x + Ut)/\delta)$ with $H(x)$ being a periodic
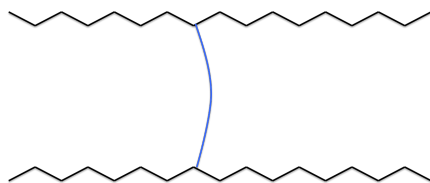
Fig. 5.3. *The channel with serrated boundaries.*



(a) $\delta = 0.04$                    (b) $\delta = 0.008$
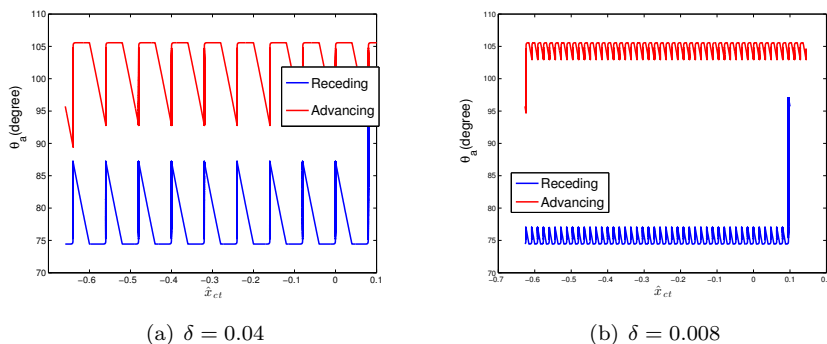
Fig. 5.4. *Contact angle hysteresis on a rough boundary with a serrated shape.*

function with period 2:

$$H(x) = \left\{ \begin{array}{ll} kx & 0 < x < 1, \\ -kx & 1 < x < 2. \end{array} \right.$$

Here we let $k = \tan(\pi/12)$. We choose the static Young's angle to be $\theta_Y = \pi/2$ and $U = \pm 0.01$. Notice that the function $h(x,t)$ is not differentiable at some points. But we still can solve the ODE system (4.12) numerically by setting $H'(x)$ to be its left or right limit of $H'$ at these points. The numerical results are similar to that in the previous example. We show only a few results in Figure 5.4 for the choices that $\delta = 0.04$ and $\delta = 0.008$. We could see the obvious contact angle hysteresis phenomena. When $\delta = 0.04$, we could see clear stick-slip behaviour from the trajectories. At some points, the contact points is pinned while the contact angle changes. The slip occurs with dramatic changes of both the contact position and the contact angle. Furthermore, numerical results indicate that the stick-slip behaviour occurs only on the discontinuous points of the boundary. For example, the contact point on the lower boundary is pinned only at highest vertexes of the surface and slips at lowest points. From the case $\delta = 0.008$, we could see the advancing angle is about $7\pi/12 = 105^o$ and the receding angle $5\pi/12 = 75^o$, which could be described again by the modified Wenzel's equation, noticing that $\theta_Y = \pi/2$ and $\theta_g = \pi/12$ in this case.

*Example 3.* In the third example, we consider the effect of the velocity. Suppose the rough boundary are similar to that in Example 1. Here, we choose $\delta = 0.002$ and $\theta_Y = 2\pi/3$. We solve the problem (4.12) with different velocity $U$. The numerical results are shown in Figure 5.5. We could see that with increasing velocity, the advancing angle becomes larger and the receding angle becomes smaller. The changes of the contact angle are almost symmetric although the decreasing of the contact angle seems slightly faster.
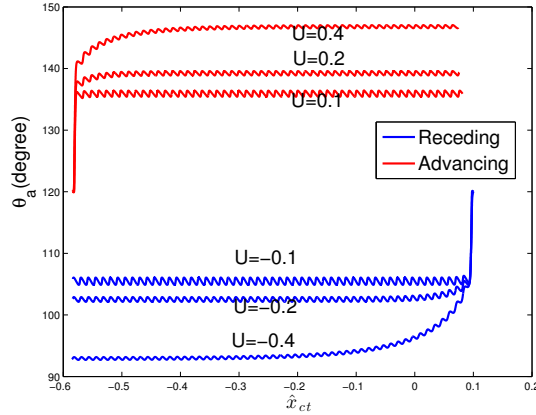
FIG. 5.5. *Velocity dependence of the contact angle hysteresis in Example 3(with relatively small velocity).*

*Example 4.* In the last example, we consider the velocity dependence of the contact angle hysteresis on a chemically patterned surface. In this calculation, we consider a flat boundary $h = 0.5$ and assume $\theta_Y(x)$ is a periodic function with period 0.2. In each period, $\theta_Y(x)$ is equal to $3\pi/4$ in a half of the period and $9\pi/10$ in the other half. We consider several choices of the velocity. The velocity are relatively larger than that in previous cases. The numerical results are shown the left subfigure of Figure 5.6. In this case, we could see the asymmetry of the velocity dependence of the contact angles, which means that the change of the advancing and receding contact angles are different with increasing velocity. This phenomena occurs since the velocity is relatively large and the asymmetry choice of the Young's angles. If the Young's angles of the chemically patterned surface are symmetric with respect to $\frac{\pi}{2}$, the velocity dependence of the advancing and receding angles is also symmetric. In addition, if the velocity is small, the asymmetry of the velocity dependence is not obvious, as in the previous example.

Interestingly, the similar asymmetry of the velocity dependence of the contact angle hysteresis has been observed in experiments, see the right subfigure in [12]. We could see that the numerical results looks similar to that in physical experiments. This indicates that the ODE system captures some essential feature of contact angle hysteresis. However, we would like to remark that the numerical results do not match the experiments quantitatively. There are many reasons for that. One obvious one is that the geometric setups are not the same. In our case, we simply consider a channel with rough boundary. In the physical experiments, they considered a fibre pulling out and pushing into a liquid bath.

**6. Conclusions.** We study the dynamic contact angle hysteresis by using a phase-field equation with a relaxed boundary condition on rough surfaces. By asymptotic analysis, we derive a nonlinear ordinary differential system for the apparent contact angle and the contact point. The system can be used to understand some typical phenomena for CAH, including the asymmetry of the dependence of the advancing and receding contact angles on the velocity, which is observed in experiments recently. Some observations are obtained from our numerical examples. First, the

(a) Numerical results

(b) Experimental results([12])
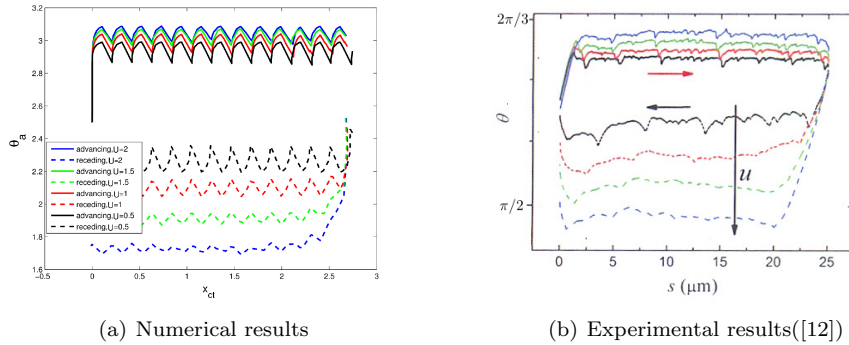
Fig. 5.6. *Non-symmetric of velocity dependence of contact angle hysteresis in Example 4(with relatively large velocity).*

advancing and receding contact angles can be characterised by the modified Wenzel or Cassie equations[27] when the velocity of the two-phase interface is small, as in quasi-static wetting problem. Secondly, the asymmetry of the velocity dependence of the CAH is induced by the asymmetry of the chemical or geometric properties of the solid surface. It is obvious for only relatively large velocities.

We remark that we do not consider the fluid effects in our study. The dissipation in the fluid might be important to quantify the contact angle hysteresis especially when the fluid velocity is large. Although numerical simulations are possible as in[24, 20], theoretical analysis for that problem will be much more difficult. A recent developed strategy by using the Onsager principle as an approximation tool might be useful for the analysis[28, 9]. This will be left for future study.

## REFERENCES

[1] G. Alberti and A. DeSimone. Quasistatic evolution of sessile drops and contact angle hysteresis. *Archive for rational mechanics and analysis*, 202(1):295–348, 2011.

[2] A. L. Bertozzi. The mathematics of moving contact lines in thin liquid films. *Notices of the AMS*, 45(6):689–697, 1998.

[3] D. Bonn, J. Eggers, J. Indekeu, J. Meunier, and E. Rolley. Wetting and spreading. *Rev. Mod. Phys.*, 81:739–805, 2009.

[4] L. A. Caffarelli and A. Mellet. Capillary drops: contact angle hysteresis and sticking drops. *Calculus of Variations and Partial Differential Equations*, 29(2):141–160, 2007.

[5] X. Chen, X.-P. Wang, and X. Xu. Analysis of the cahn-hilliard equation with relaxation boundary condition modelling contact angle. *Arch. Rational Mech. Anal.*, 213:1–24, 2014.

[6] P.G. de Gennes. Wetting: Statics and dynamics. *Rev. Mod. Phys.*, 57:827–863, 1985.

[7] P.G. de Gennes, F. Brochard-Wyart, and D. Quere. *Capillarity and Wetting Phenomena*. Springer Berlin, 2003.

[8] A. DeSimone, N. Gruenewald, and F. Otto. A new model for contact angle hysteresis. *Networks and Heterogeneous Media*, 2(2):211–225, 2007.

[9] Y. Di, X. Xu, and M. Doi. Theoretical analysis for meniscus rise of a liquid contained between a flexible film and a solid wall. *Europhysics Letters*, 113:36001, 2016.

[10] H. Y. Erbil. The debate on the dependence of apparent contact angles on drop contact area or three-phase contact line: a review. *Surface Science Reports*, 69(4):325–365, 2014.

[11] L. Gao and T. McCarthy. Contact angle hysteresis explained. *Langmuir*, 22(14):6234–6237, 2006.

[12] D. Guan, Y. Wang, E. Charlaix, and P. Tong. Asymmetric and speed-dependent capillary force hysteresis and relaxation of a suddenly stopped moving contact line. *Physical review letters*, 116(6):066102, 2016.

[13] J. F. Joanny and P.-G. De Gennes. A model for contact angle hysteresis. *The journal of*

*chemical physics*, 81(1):552–562, 1984.

[14] A. Mellet and J. Nolen. Capillary drops on a rough surface. *Interfaces Free Boundaries*, 14(2):167–184, 2012.

[15] R. Pego. Front migration in the nonlinear cahn-hilliard equation. *Proc. R. Soc. Lond., A*, 422:261–278, 1989.

[16] C. Priest, R. Sedev, and J. Ralston. Asymmetric wetting hysteresis on chemical defects. *Phys. Rev. Lett.*, 99(2):026103, 2007.

[17] C. Priest, R. Sedev, and J. Ralston. A quantitative experimental study of wetting hysteresis on discrete and continuous chemical heterogeneities. *Colloid Polym. Sci.*, 291:271–277, 2013.

[18] T. Qian, X.-P. Wang, and P. Sheng. Molecular scale contact line hydrodynamics of immiscible flows. *Phys. Rev. E*, 68:016306, 2003.

[19] R. Raj, R. Enright, Y. Zhu, S. Adera, and E. N. Wang. Unified model for contact angle hysteresis on heterogeneous and superhydrophobic surfaces. *Langmuir*, 28:15777–15788, 2012.

[20] W. Ren and W. E. Contact line dynamics on heterogeneous surfaces. *Physics of Fluids*, 23:072103, 2011.

[21] M. Reyssat and D. Quéré. Contact angle hysteresis generated by strong dilute defects. *J. Phys. Chem. B*, 113(12):3906–3909, 2009.

[22] J. Snoeijer and B. Andreotti. Moving contact lines: scales, regimes, and dynamical transitions. *Ann. Rev. Fluid Mech.*, 45, 2013.

[23] A. Turco, F. Alouges, and A. DeSimone. Wetting on rough surfaces and contact angle hysteresis: numerical experiments based on a phase field model. *ESAIM: Mathematical Modelling and Numerical Analysis*, 43(06):1027–1044, 2009.

[24] X.-P. Wang, T. Qian, and P. Sheng. Moving contact line on chemically patterned surfaces. *J. Fluid Mech.*, 605:59–78, 2008.

[25] X.-P. Wang and X. Xu. A dynamic theory for contact angle hysteresis on chemically rough surface. *Discrete and Continuous Dynamical Systems-A*, 37:1061–1073, 2017.

[26] G. Whyman, E. Bormashenko, and T. Stein. The rigorous derivation of young, cassie–baxter and wenzel equations and the analysis of the contact angle hysteresis phenomenon. *Chem. Phys. Lett.*, 450(4-6):355–359, 2008.

[27] X. Xu. Modified wenzel and cassie equation for wetting on rough surfaces. *SIAM J. Appl. Math.*, 76:2353–2374, 2016.

[28] X. Xu, Y. Di, and M. Doi. Variational method for contact line problems in sliding liquids. *Phys. Fluids*, 28:087101, 2016.

[29] X. Xu and X.-P. Wang. Analysis of wetting and contact angle hysteresis on chemically patterned surfaces. *SIAM J. Appl. Math.*, 71:1753–1779, 2011.

[30] X. Xu and X.-P. Wang. The modified cassie's equation and contact angle hysteresis. *Colloid Polym. Sci.*, 291:299–306, 2013.

[31] X. Xu and X.-P. Wang. Non-darcy behavior in two-phase channel flow. *Phys. Rev. E*, 90:023010, 2014.